Electric Field-Modulated Non-Ohmic Behavior of Carbon Nanotube Fibers in Polar Liquids

Jeronimo Terrones[†], *James A. Elliott*[†], *Juan J. Vilatela*[‡], *and Alan H. Windle*[†]*

[†]Department of Materials Science, University of Cambridge, 27 Charles Babbage Road, Cambridge, CB3 0FS, United Kingdom.

[‡]IMDEA Materials Institute, Eric Kandel 2, Getafe, Madrid 28906, Spain.

*Address correspondence to: ahw1@cam.ac.uk

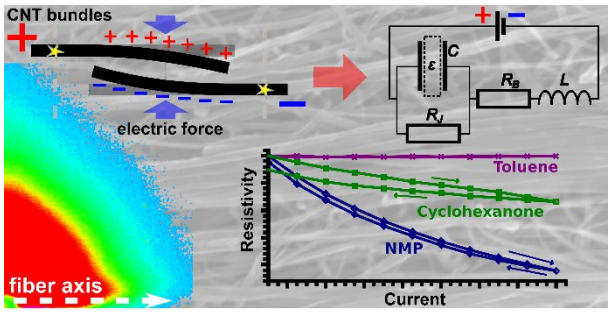

ABSTRACT: We report a previously unseen non-Ohmic effect in which the resistivity of carbon nanotube fibers immersed in polar liquids is modulated by the applied electric field. This behavior depends on the surface energy, dielectric constant, and viscosity of the immersion media. Supported by synchrotron SAXS and impedance spectroscopy, we propose a model in which the gap distance, and thus the conductance, of capacitive interbundle junctions is controlled by the applied field.

KEYWORDS: non-Ohmic effect, carbon nanotube fibers, electrical conductivity, solvent, SAXS, impedance

Most fibers made of carbon nanotubes[1–3] (CNTs), in particular those spun directly from a chemical vapor deposition (CVD) reactor,[2] have a very porous yarn-like structure.[4] The high number of contiguous pores translates into a large specific surface area (measured to be from 70 to 200 $m^2 g^{-1}$)[5,6] available for interacting with the surrounding medium. Such voids imbue these CNT fibers with a range of properties unachievable by non-porous ones. For example, the pores can be filled by a polymer to make composites in which the intimate matrix/reinforcement interaction could help translate the superb mechanical properties of the CNTs to the macroscale;[6,7] or used to carry functional (superconducting, catalytic, sensing) powders to make textiles of materials impossible to weave by themselves.[8,9] However, it is first necessary to understand the fiber/medium interactions in detail in order to unleash the full potential of CNT fibers, and similar hierarchical assemblies, in applications as diverse as high-performance multifunctional composites,[6–11] sensors and actuators,[8,12–15] or energy transmission and storage.[16–19]

In previous work,[5] we reported the effects of several penetrant liquids on the structure and electrical properties of direct-spun CNT fibers. We found that, upon immersion in the liquid, the fiber assumes a different, more energetically favorable, slightly swollen structure. For the liquids tested, the energetic cost of creating nanotube/liquid interface was lower than that of the nanotube/air interface, which resulted in nanotube bundle junctions springing apart to release the elastic energy required to bend bundles around obstacles to close the junction. This structural

change was observed by small angle X-ray scattering (SAXS) as a reduction of both the average pore size and the axial alignment of the bundles, and by direct current (DC) four-probe measurements, as an increase of resistivity. Wide angle X-ray scattering (WAXS) showed that liquids tested do not intercalate between nanotubes inside a bundle: their penetration is restricted to interbundle pores.

In the present article, we focus on the effect of increasing the probe current (or voltage) of the four-probe circuit while samples are already immersed in a liquid. We complement four-probe DC electrical measurements with alternating current (AC) impedance analyses in the 0.1 – 10 kHz range and SAXS from a synchrotron source to show that, when fibers are immersed in polar liquids, electrostatic forces due to charge accumulation at open junctions can, at least partially, reverse the effect of liquid infiltration. These forces bring the bundles in the junctions closer together, or even completely close junctions, thus reducing the resistance of the fiber samples. This effect not only gives us a better insight on the structure/property relations of CNT fibers and related assemblies but could also be exploited in sensing or measuring devices.

RESULTS AND DISCUSSION

Carbon Nanotube Fibers. The CNT fibers used in this study were produced by the direct CVD spinning method, originally developed over a decade ago.[2] The samples were produced using methane as the carbon source. They have diameters between 10 and 15 μm, a surface area of 75.6 $m^2 g^{-1}$, and a porosity of 54%. They are composed of nanotube bundles with diameters in the range 20 to 30 nm, and pores in the range 30 to 40 nm. To check for reproducibility, several experiments were carried on fibers made from other carbon sources either in Cambridge or in a similar reactor at the IMDEA Materials Institute in Madrid.[20] There appeared to be no

statistically significant difference between fibers with densities in the range 0.2 to 0.6 g cm^{-3}. As can be seen in Figure 1(a-c), fibers made by this method have a porous hierarchical structure consisting of a network of close packed bundles of CNTs preferentially aligned to the fiber axis direction. The specific characteristics of the nanotubes building-up the bundles depend on the carbon source and other synthesis parameters; they may be single-, double-, or multi-walled and, depending on their diameter, they may have a collapsed "dog bone" structure.[21–23] Figure 1d shows a 2D schematic of the conductive bundle network that makes up the fiber and the effect that immersion in a liquid has on its structure: when the specific bundle/liquid interfacial energy, $\gamma_{b/l}$, is lower than that for the bundle/air interface, $\gamma_{b/a}$, bundle junctions spring open resulting in a slightly swollen and less conductive fiber with an increased number of pores with a smaller average pore diameter. The figure does not show the effects of the liquid on bundle alignment; for a more detailed discussion, the reader is referred to our previous work.[5]

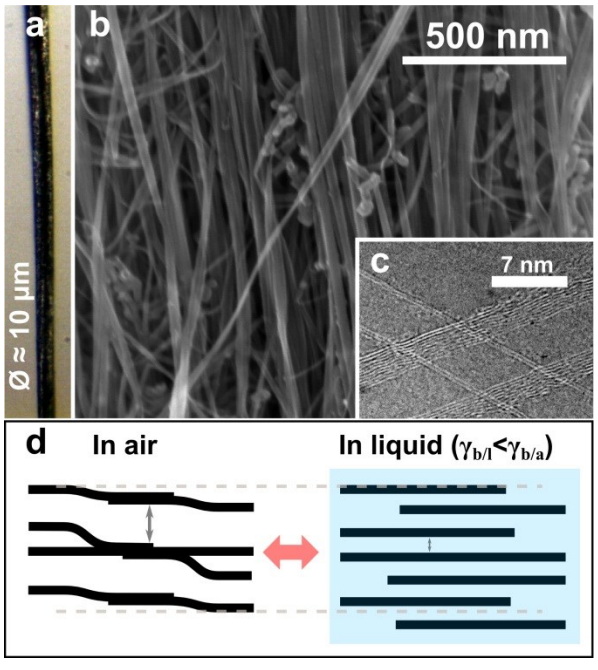

Figure 1. The hierarchical structure of direct-spun carbon nanotube fibers: (a) optical microscopy image showing the macroscopic appearance fibers used in this work; (b) scanning

electron microscopy (SEM) image of the same fiber showing the network of nanotube bundles; (c) transmission electron microscopy (TEM) image showing the individual nanotubes that make up the bundles. (d) Schematic of the effects of liquid immersion on the structure and connectivity of the CNT bundle network (where $\gamma_{b/l}$ is the specific bundle/liquid interfacial energy and $\gamma_{b/a}$ is that for the bundle/air interface).

Effect of Varying the Electric Field. When fibers were immersed in polar liquids (cyclohexanol, ethanol, methanol, cyclohexanone, acetone, and *N*-methyl-2-pyrrolidone), it was observed that increasing the current (or voltage) of the four-probe circuit reduced their electrical resistance; reducing the current made the resistance rise again. This unexpected non-Ohmic behavior was not observed in the non-polar liquids tested (cyclohexane, carbon tetrachloride, and toluene), in which resistance didn't change, nor in air, where a small increase was observed when increasing current. Figure 2 summarizes the observed behavior. The modulation of resistance was reversible, despite some hysteresis that reduced gradually after cycling the current (see dashed lines in Figure 2a and section 9 of the Supporting Information). More importantly, the change in resistance did not occur instantaneously: once the current was changed, it took some time for the resistance to reach its new value. The direct spun CNT fibers generally have a metallic behavior around room temperature, with a positive thermal coefficient of resistance (see section 1 of Supporting Information) so any Joule heating of the material due to increasing current would be expected to increase the resistance (as seen for air in Figure 2b), not reduce it, thus ruling out a possible thermal effect as the cause of the phenomenon. Since most of the resistance of a macroscopic CNT assembly is thought to originate from interbundle junctions,[24] this effect could potentially be attributed to liquid molecules re-arranging due to electric fields at such junctions. However, it took the fibers immersed in *N*-methyl-2-pyrrolidone (NMP), the

medium which produced the fastest responses, a few seconds to reach their new stable resistances. These response times are far slower than the characteristic times of dielectric relaxation (between 10^{-10} and 10^{-2} seconds) thus also ruling out this scenario.

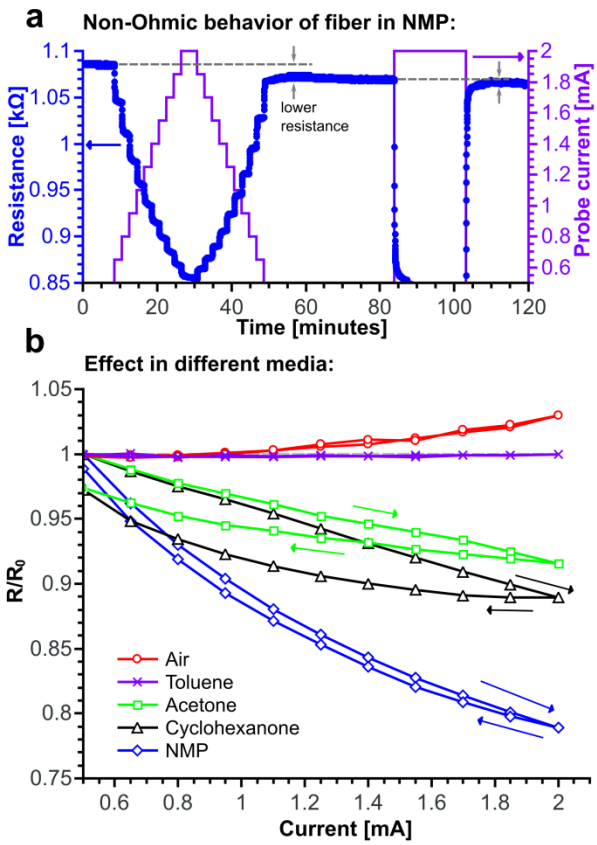

Figure 2. Observation of the non-Ohmic behavior in direct spun CNT fibers: (a) resistance (left axis) of a fiber immersed in *N*-methyl-2-pyrrolidone (NMP) is modulated by the applied probe current (right axis); the horizontal dashed lines indicate a reduction of hysteresis after cycling the current. (b) Relative change in resistance (compared to fiber in air at 0.5 mA, R_0) as a function of probe current for fibers in air and 4 liquids; a reduction in resistance with increasing current occurs only in the 3 polar liquids.

For different polar liquids tested on identical fibers, the average changes in resistance when increasing current from 0.5 to 2.0 mA were as follows: –5% for ethanol, –9% for acetone, –11%

for cyclohexanone, and −21% for NMP. These trends are very similar to those observed previously[5] for the resistance increase when immersing the fibers in the same liquids [ethanol (+10%), cyclohexanone (21%), acetone (23%), and NMP (+38%)]. In the associated discussion, we had ascribed the time-delayed increases in resistance upon immersion to the opening of bundle junctions due to a change of the medium/nanotube interfacial energy, γ, when changing the medium from air to liquid. Hence, a consistent explanation for the newly discovered non-Ohmic behavior is that electromagnetic forces induced by the increase of current or electric field partially reverse the effect of liquid infiltration: closing junctions or, at least, bringing bundles in an open junction closer together.

Dependence on Viscosity. To investigate the dependence of the resistive response on viscosity, the reaction times of the fiber were measured in a single liquid at several temperatures and then compared them to the shear viscosity, η, of the liquid measured in the same temperature range. With possible applications in composites in mind, we selected a low viscosity epoxy resin (without any hardener) based on the diglycidyl ether of bisphenol A (DGEBA) that has a similar but slower effect on the resistance of the fibers as the other polar liquids. Figure 3 summarizes the results for CNT fibers immersed in DGEBA. We define the relative resistance as $\frac{R_0-R}{R_0-R_{final}}$; where R is the resistance, R_0 is the resistance at t_0 (the moment where current is stepped up or down), and R_{final} is the resistance after the system stabilized (approximately 2 hours were given to the system to stabilize). In this way, the relative resistance change is always positive and spans from zero to unity. We also define a 'characteristic time', τ, as the time (measured from t_0) that it took the fibers to reach a relative resistance of 0.632 (*i.e* $1-e^{-1}$). Figure 3a shows the resistance change as a function of time for a single fiber at several temperatures when the current was increased from 0.5 to 2.0 mA; the time constants reduced from 320 s at 30 °C to 20 s at

100 °C. In Figure 3b, the time constants of the immersed fiber (results for 3 samples shown) are compared to the viscosity of the pure resin, as measured by a rotating plate rheometer while being heated and cooled in the same temperature range. Both quantities are expected to follow Arrhenius relationships of the form:

$$\vartheta = \vartheta_0 e^{\frac{E_\vartheta}{RT}} \quad (1)$$

where ϑ is either the time constant, τ, or the viscosity, η; ϑ_0, to be replaced by τ_0 or η_0, is a constant; E_ϑ is the activation energy of some characteristic process of the system; R is the universal gas constant; and T is the absolute temperature. The average E_τ of the six samples measured was 35±3 kJ mol^{-1}. E_η has a value of approximately 33 kJ mol^{-1} for temperatures higher than 37 °C (1/T ~ 0.0032 K^{-1}); at lower temperatures it increased to ~55 kJ mol^{-1}. To within the statistical errors in the data, we can conclude that, in the higher temperature regime, E_τ=E_η and thus the characteristic response time of the fibers follows the same relationship with temperature as the viscosity of the immersion medium. This is significant because it supports the hypothesis that the re-arrangement of CNT bundles, at a rate limited by the viscous flow of resin, is the cause of the non-Ohmic phenomenon.

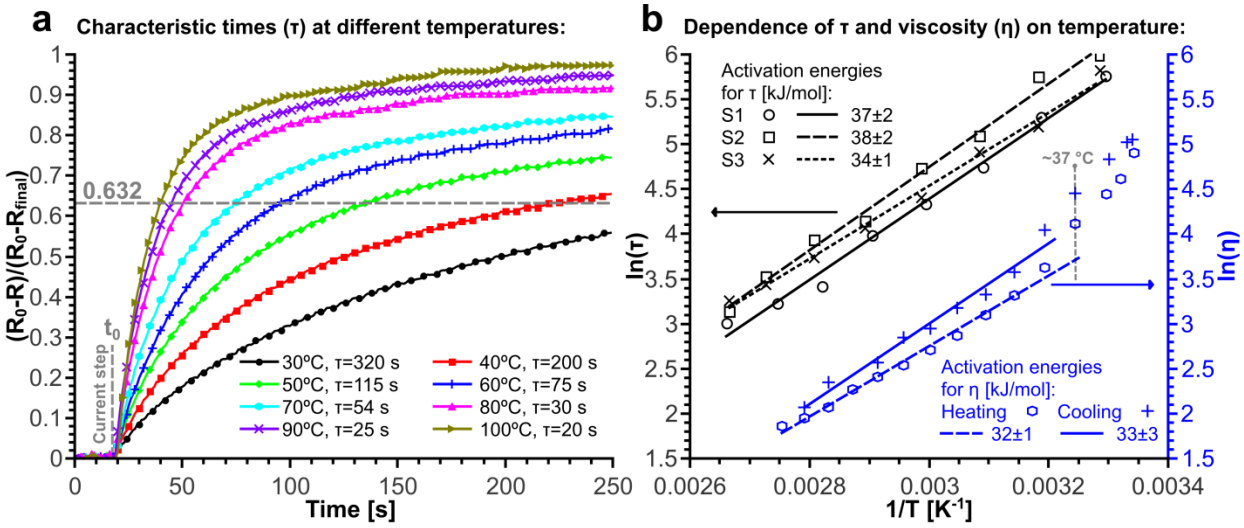

Figure 3. Dependence of non-Ohmic behavior on viscosity of DGEBA-based epoxy resin (no hardener added): (a) relative resistance change as a function of time (at t_0, probe current is stepped from 0.5 mA to 2.0 mA) at different temperatures; the 'characteristic time', τ, as defined in text, and determined from an Arrhenius fit, is shown for the different temperatures. (b) Dependence of τ and the shear viscosity of the pure resin, η, on temperature: both follow Arrhenius relationships with activation energies of approximately 35 kJ mol^{-1}. The low-temperature ($T < 310$ K, $1/T \sim 0.0032$ K^{-1}) behavior of viscosity (with activation energies of approximately 55 kJ mol^{-1}) is believed to be due to incipient crystallization of the resin and is discussed further in the text.

The observed behavior for η in the low temperature regime, but absent for τ, may give further clues to the origin of the non-Ohmic effect. Epoxy resins are supercooled liquids with melting points of approximately 40 °C; at lower temperatures they tend to slowly crystallize. We propose that the observed change of the resin to a more viscous regime (as measured by the rheometer) is due to the formation of microscopic crystals that macroscopically thicken the liquid. When measuring the time constants of the fiber samples however, we are measuring the movement of nanometer-sized entities in nanometer-sized pores (both ~30 nm in diameter) where the microcrystals cannot penetrate; thus τ is insensitive to the macroscopic change of regime. Speculatively, the changes in fiber resistance could be used to monitor resin infiltration in large fiber arrays during composite fabrication by infusion processes such as resin transfer molding (RTM).

Comparison of Electromagnetic Forces. We have, so far, presented evidence that bundles within the fiber move under the influence of electromagnetic forces at higher probe currents. There are two forces which could play an important role in moving the bundles closer together.

The first is an electrostatic force due to charge accumulation in open junctions, analogous to the force between the plates of a capacitor, of the form:

$$F_C = \frac{\varepsilon A V^2}{2 d_C^2} \tag{2}$$

where ε is the permittivity of the medium, A is the area of the junction, V is the potential drop at the junction, and d_C is the separation between the surfaces of the bundles at the junction. The second is an electrodynamic force, due to current flowing through parallel paths, of the form:

$$F_L = \frac{\mu l_L I^2}{2 \pi d_L} \tag{3}$$

where μ is the permeability of the medium, l_L is the length of the conducting path, I is the current flowing through the paths, and d_L is the separation. The quotient of equations 2 and 3 gives:

$$\frac{F_C}{F_L} = \frac{\pi\varepsilon}{\mu} \cdot \frac{d_L l_C D}{l_L d_C^2} \cdot \frac{V^2}{I^2} \tag{4}$$

where we have already replaced $A = D \cdot l_C$ (the diameter of the bundle times the length of the junction) for the area of the junction. The first term of the product only contains constants, known for each medium; the second, geometric factors; and the third, electric parameters. From our knowledge of the geometry of the junctions we can set: $D = 30$ nm; $l_C = 50$ nm, a length comparable to the pore sizes determined in our previous work;[5] $d_L = 60$ nm, the distance between the centers of two bundles 30 nm apart; $d_C = 35$ nm, a separation accounting for the curvature of the bundles; and $l_L = 1$ cm, the length of an entire sample – since the electrodynamic force is not local to the junction but extends along the whole current path. To determine the electric parameters, we will consider a typical fiber sample with a resistance of 1 kΩ and a current of 1 mA flowing through it. At any point, the cross section of a fiber contains around sixty thousand bundles; implying 6×10^4 parallel conducting paths and a current of 1.6×10^{-8} A per path. The nanotubes in our fibers are about 1 mm long[22,25] and one would expect

the close-packed bundles to be at least as long. Making an allowance for misalignment, it would take around 20 bundles to cover the 1 cm length of our fiber samples: or around 20 junctions cm^{-1} per conducting path. With the reasonable assumption that most of the voltage drops along the conducting path occur at junctions,[24] we have a drop of 0.05 V at each junction. Substituting the previous values in equation 4 yields:

$$\frac{F_C}{F_L} \approx 10^3 \varepsilon_r \tag{5}$$

where ε_r is the relative permittivity of the medium and we are ignoring a factor of μ_r^{-1}, the relative magnetic permeability, because the deviation from the permeability of vacuum is ~10^{-6} for all the tested media.[26] Since $\varepsilon_r \geq 1$, we can conclude that the electrostatic force, being at least 3 orders of magnitude greater than the electrodynamic one, dominates the behavior of the fiber. This result explains why the non-Ohmic phenomenon is observed only in polar liquids: their dielectric constants are at least 10 times larger than those of non-polar liquids (see table S1 in Supporting Information) and so the electrostatic force forces the bundles closer together. In fact, a correlation was found between the product of the dielectric constant of the liquid with the resistance increase upon immersion at low currents (related to the number of open interbundle junctions) and the resistance decrease when switching to high currents (see section 8 of the Supporting Information).

Model Explaining Observed Behavior. Figure 4a shows a schematic of a bundle junction; the yellow stars represent points at which the CNT bundles cannot move due to entanglements or other obstacles. Figure 4b presents the equivalent circuit for such system. The junction behaves as a leaky capacitor (*i.e.* a capacitor with a resistor in parallel): as the current through (or voltage at) the junctions is increased, charge accumulation increases the force between the "capacitor plates", bringing the bundles closer together and reducing the junction's resistance, R_J. The

series resistor, R_B, and inductor L, represent the finite resistance and self-inductance of the bundles outside the junction. The mechanical force, resulting from bending the bundles opposes the electrostatic force, and a new equilibrium distance, d_{eq}, is reached. A preliminary model in which bundles are assumed to deflect as cantilever beams allowed us to get an approximate idea of the changes in d_{eq} as a function of applied voltage (by equating the cantilever equation, see eqn. S1, to equation 2). Figure 4c shows experimental *R* vs *V* data of fibers immersed in acetone (symbols) and a curve fittings using our approximation of d_{eq} (lines). Solid lines are the best fits for a model that assumes an exponential dependence of resistance on distance of the form:

$$R_T \approx e^{\frac{d_{eq}}{\lambda}} \tag{6}$$

where λ is a characteristic length ruling how fast the resistance grows; a behavior characteristic of tunneling conduction.[27] Dashed lines represent the expected behavior of resistance if conduction through a junction had the diffusive nature of the Drude model (*i.e.* a resistance directly proportional to bundle separation). It is clear that the Drude model will fail to predict the observed behavior no matter how much fine tuning is carried on, it predicts a curvature opposite to that observed experimentally. Electron tunneling through the interbundle gaps seems to be the dominant conduction mechanism. A more detailed quantitative model of this phenomenon is currently in preparation.

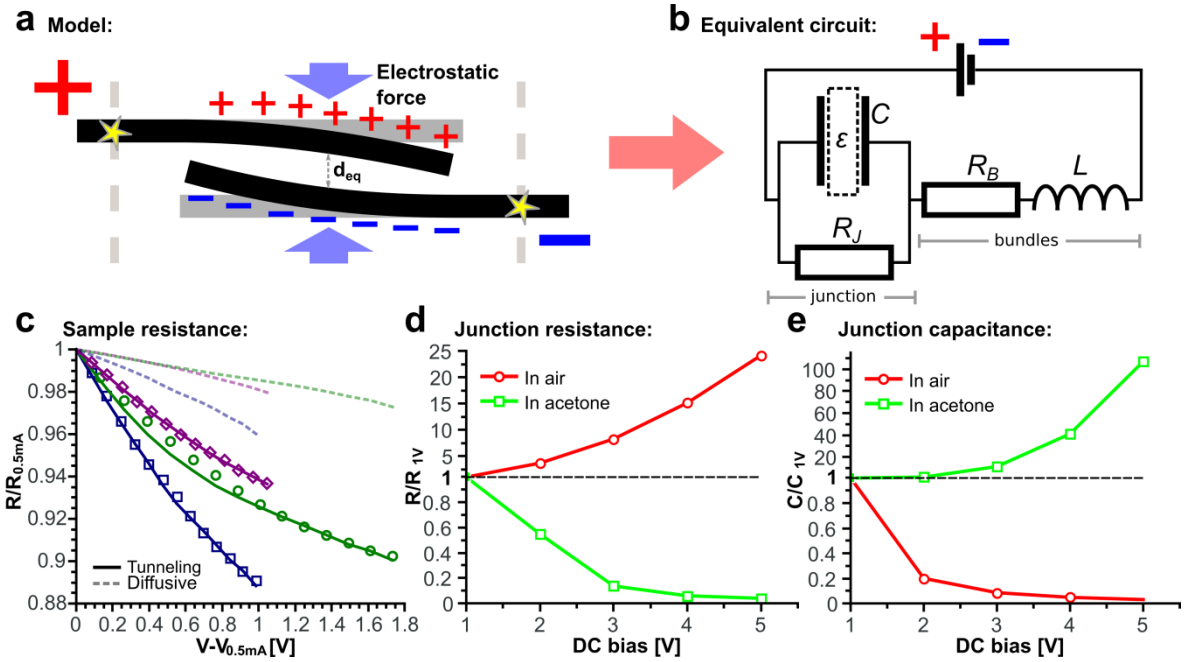

Figure 4. Model for electrical conductivity of CNT fibers: (a) and (b) an open bundle junction behaves like a leaky capacitor: as the probe voltage (or current) is increased, charge accumulation generates an electrostatic force that bends bundles closer together thus reducing junction resistance. The equilibrium distance of the junction, d_{eq}, will be that at which the electrostatic force is equal and opposite to the elastic force resulting from bending the bundles. The series elements in (b) represent the self-inductance and resistance of the bundles away from the junction. (c) Comparison of the predictions of two conduction models (lines) to experimental data (symbols) for three fiber samples: dashed lines represent the "conventional" Drude model in which the resistance of the junction is linearly related to the predicted equilibrium distance, solid lines assume the exponential dependence on distance characteristic of tunneling conduction. Change in characteristic resistance (d) and capacitance (e) as a function of applied bias voltage obtained from impedance experiments; dashed lines indicate a change in the scale of y axes. Values were obtained by using the equivalent circuit of (b) to fit reactance (imaginary component of impedance) data in the 0.1 to 10 kHz frequency range. The increase in capacitance

and decrease in resistance observed in fibers immersed in acetone agrees with the proposed model of a capacitive junction with a field-dependent equilibrium distance. The opposite behavior of the fiber in air can be attributed to Joule heating of the junctions.

Impedance Measurements. From the effective medium approximation,[28–30] it follows that we can use the equivalent circuit for a single junction to obtain characteristic parameters of the entire fiber network system. The reactance (imaginary component of impedance), X, of the circuit presented in Figure 4b is given by:

$$X = \omega L - \frac{\omega C R_J^2}{1+(\omega C R_J)^2} \tag{7}$$

where ω is the angular frequency of the applied voltage and the other symbols correspond to those in Figure 4b. To extract the characteristic parameters, we measured the impedance of samples in air and immersed in acetone in the 0.1 – 10 kHz range while applying DC bias voltages from 1 V to 5 V and fitted equation 7 to the reactance data (see section 5 of Supporting Information). Our results are summarized in Figures 4d and 4e, where we compare changes in characteristic junction resistance and characteristic junction capacitance (relative to their values for a bias of 1 V) as a function of bias voltage; note the changes in the *y*-scale below and above unity. When the CNT fibers were immersed in acetone, increasing the voltage reduced the characteristic resistance and increased its capacitance; whereas the complete opposite effect is observed in air. The effect in acetone is congruent with our models since either a reduction in the gap distance or a full collapse of a junction will result in a reduction of resistance and an increase in capacitance (the capacitance will not vanish when junctions are closed because there will always be a resistance of ~3 MΩ associated with the contact[24]). The effect in air is consistent with Joule heating of the junctions, especially closed ones: the increase in resistance agrees with the positive thermal resistivity coefficient of the fibers, and the reduction in capacitance is

consistent with the heating of the dielectric (mainly polymeric byproducts of the synthesis process[31]) between bundles in closed junctions.

Although the relative increase in characteristic resistance with increasing DC bias appears to be rather high (a factor of 25 under 5 V applied bias), this should not be interpreted as being directly related to the increase of overall DC resistance of fiber itself (usually less than 10% but dependent on fiber composition and morphology). This is because the overall resistance of fiber will be dominated by a limited number of paths of least resistance,[32] whereas the characteristic resistance measures the changes in AC behavior of all of the junctions in the fiber, whether or not they contribute significantly to the overall DC conduction pathway. More extensive studies of the characteristic resistance and capacitance of fiber network are underway, and will be reported in a subsequent publication.

Small-Angle X-Ray Scattering. The effect of voltage on the shape of the network of conductive elements that make the fibres was determined by *in situ* synchrotron small-angle X-ray (SAXS) measurements on fibres immersed in capillaries filled up with NMP (experimental details in section 6 of Supporting Information) and subjected to different voltages. From the 2D SAXS pattern, we integrated scattering intensity radially in a q range of 0.2 – 1.2 nm^{-1} and plotted this value against azimuthal angle. The full-width-at-half-maximum (FWHM) of this azimuthal profile provides a measure of the degree of orientation of CNTs and bundles in the fibre. The FWHM values against applied voltage are plotted in Figure 5, which also includes a typical pattern and an SEM image of the fiber for reference (insert to Figure 5). The plot shows an overall drop in the FWHM with increasing applied voltage, maintained even after the voltage is off and indicating an increase in CNT alignment parallel to each other and to the fibre axis. Such an improvement in orientation implies a closer contact between elements in the fibre

through better packing and a reduction in the distance between them, and is thus consistent with the similar drop in electrical resistance. Note also that since the improvement in orientation is preserved after the voltage is off, the application of an electric filed works in fact as a conditioning method that could be used to lower longitudinal electrical resistance of CNT fibres/epoxy composites. The 2D SAXS measurements also confirm the trend in Figure 3 showing a gradual drop in electrical resistance with a time constant that depends on viscosity of the liquid. An equivalent time correspondence with our synchrotron measurements cannot be established because the individual patterns, with exposure time of 1 s, are too weak, but by comparing two averages of 10 patterns, one just upon voltage application and another before switching it off, we observe a decrease of a few degrees in the FWHM.

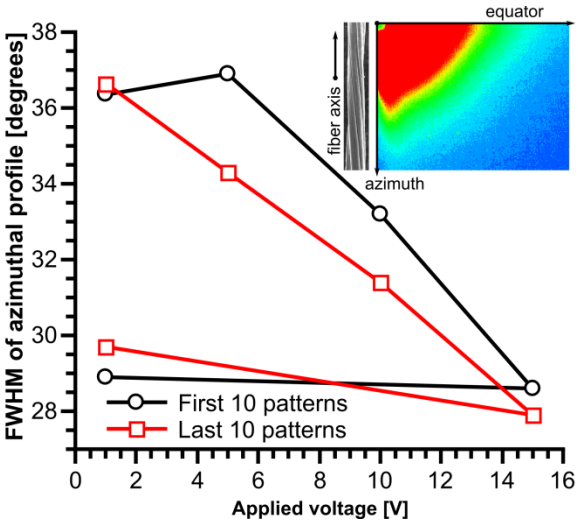

Figure 5. FWHM of the azimuthal profile of 2D SAXS patterns of a fiber immersed in NMP and subjected to different voltages. The black line corresponds to the sum of the first ten 1 s patterns (of a series of 100) and the red line to the last ten. The differences between these two traces are due to the finite time required for the structural change to take place. The insert shows an example 2D pattern and an SEM image of a typical fiber sample.

CONCLUSIONS

To summarize, we have demonstrated non-Ohmic resistive behavior in macroscopic CNT fibers infiltrated with polar liquids or polymers. This behavior is ascribed to the much higher dielectric constant of these media relative to air (*i.e.* fiber before infiltration) or non-polar liquids. When using low viscosity epoxy as infiltrating medium, we find the temperature dependence of both resin viscosity and electrical resistance to lead to very similar activations energies. This suggests that the non-Ohmic behavior in infiltrated fibers is due to the reshaping of the CNT network in the fiber, induced by the electric field at the capacitive bundle junctions and detectable as an increase in bundle orientation as measured by synchrotron SAXS. The combination of resistive and capacitive behavior in the fiber is confirmed by impedance spectroscopy on dry and infiltrated fibers. For infiltrated fibers, impedance results point to an equivalent circuit that includes capacitive junctions with field-dependent equilibrium distance. Dry fibers (*i.e.* non-infiltrated) show only the effects of Joule heating of the junctions.

The non-Ohmic behavior in CNT fibers is ultimately a manifestation of nanoscale effects, for example conduction by inter-junction tunneling, detectable on a macroscopic length scale. While we do not expect that this behavior is unique to CNT fibers, they are the first example known to us where such behavior is due to changes in structure on meso- and nano-scales. Thus, we anticipate that the results discussed here will apply to a variety of emerging hierarchical structures made up of other nanobuilding blocks assembled into macroscopic materials, such as graphene fibers, nanowire membranes, self-assembled metamaterials and various other macroscopic hybrid materials.

MATERIALS AND METHODS

Direct CVD Fiber Spinning. The carbon nanotube fibers used in this work were produced by the direct chemical vapor deposition (CVD) spinning method developed around 2004 in the Department of Materials Science of the University of Cambridge.[2] In this method a carbon source (methane, ethanol, toluene, or other hydrocarbon), a precursor for iron particles (ferrocene), and a growth promoter (usually thiophene) are pyrolyzed at 1300 °C in a tubular reactor under a hydrogen atmosphere. The reaction forms an elastic "CNT aerogel" that is then pulled out from the furnace, densified with an acetone mist, and wound onto a spool as a fiber.

Liquids Used as Immersion Media. All the solvents used in this experiment were bought from Sigma-Aldrich; their specifications are as follows: acetone (ACS reagent ≥99.5%), carbon tetrachloride (reagent grade ≥99.9%), cyclohexane (ACS reagent ≥99%), cyclohexanone (ACS reagent ≥99%), cyclohexanol (Reagent Plus 99%), ethanol (ACS reagent ≥99.5%), methanol (laboratory reagent ≥99.6%), n-methyl-2-pyrrolidone (CROMASOLV Plus ≥99%), and toluene (ACS reagent ≥99.5%). The DGEBA-based resin used for the viscosity dependence experiment was that of the RT151 low viscosity epoxy resin system from ResinTech Ltd. Table S1 (Supporting Information) lists the molecular dipole moments and relative dielectric constants of the immersion media.

Direct Current Measurements. A custom-built four probe circuit was used to monitor the resistance of the fiber samples; the device has a variable current supply providing from 0.005±0.002 mA to 2.000±0.002 mA, a voltmeter with a sensitivity of 1 mV, and a maximum sampling frequency of 10 Hz. Samples already mounted in a sample holder were connected to the circuit (with an initial probe current of 0.5 mA) and placed inside a beaker. The liquid to be tested was slowly poured into the beaker until it covered the fiber. A sufficiently long time

(which varied depending on the liquid) was waited until the resistance stabilized. After all the resistance changes reported in our previous paper[5] took place and the resistance had a stable value, the probe current was increased to 2.0 mA; this was done either in a single or multiple steps waiting for the resistance to stabilize after each step. Once the resistance was stable at 2.0 mA, the current was taken down back to 0.5 mA. The same procedure was used for the experiment exploring the dependence of the resistive behavior on the viscosity of the liquid, but the beaker was immersed in a heated silicone oil bath to change the temperature. Further details of sample mounting can be found in section 3 of Supporting Information.

Rheology. An AR2000EX rotating disc rheometer from TA Instruments was used to determine the viscosity of the DGEBA epoxy resin in the 30 to 100 °C range, both while heating up and cooling down the liquid.

Alternating Current Measurements. A ModuLab system from Solartron Analytical was used in a four-probe configuration to measure the impedance of our samples in the 100 Hz – 10 kHz range at various DC bias voltages. The starting frequency was chosen to be high enough not to interfere with the expected structural changes in the fiber (with characteristic times of more than one second). Immersed samples were first taken to a fixed DC bias (from 1 to 5 volts) and a sufficient time was waited for their resistances to stabilize; then the AC frequency sweep was carried with a RMS amplitude of 0.5 V. Samples were mounted the same way as for DC measurements (section 3 of Supporting Information). Details of the data analyses can be found in section 5 of Supporting Information.

Small-Angle X-Ray Scattering. XRD measurements were performed at the Non-crystalline Diffraction beam line at Alba Light Source using a wavelength of 1Å. Samples were mounted in a modified version of our sample holders with only two electrical contacts and a sealed

Lindemann glass capillary filled with the tested liquid, as shown in Figure S4 (Supporting Information). To get a stronger SAXS signal, thicker samples (equivalent to 30 normal fibers) were used. DC potential differences ranging from 1 to 15 V were applied while capturing a 2D SAXS pattern every second. Further details on sample mounting and data analyses are available in section 6 of Supporting Information.

AUTHOR INFORMATION

Corresponding Author

*Address correspondence to: ahw1@cam.ac.uk

Conflict of Interest Disclosure

The authors declare no competing financial interest.

ACKNOWLEDGMENT

The authors are grateful to H. Yue and J. P. Fernandez for their assistance with synchrotron and rheological measurements, and to T. Gspann for the SEM image of figure 4. JT acknowledges generous financial support from: The Cambridge Commonwealth European and International Trust, CONACyT (Mexico), Dyson Ltd, and Pembroke College Cambridge. JJV acknowledges support from MINECO (Spain) and FP7-People-Marie Curie Action-CIG. Synchrotron XRD experiments were performed at NCD beam line at ALBA Synchrotron Light Facility with the collaboration of ALBA staff.

ASSOCIATED CONTENT

Supporting Information.

Supporting Information Available: Additional details on CNT fibers and their temperature coefficient of resistance, liquids used as immersion media, four-probe sample mounting, the balance of electrical and elastic forces, AC analysis, synchrotron experiments, the resistive behavior of conventional carbon fiber at various currents, the correlation between dielectric constant and resistance reduction in CNT fibers, and the hysteresis of the non-Ohmic behavior are included in the supporting information. This material is available free of charge *via* the Internet at http://pubs.acs.org.

ABBREVIATIONS

2D, two-dimensional; AC, alternating current; CNT, carbon nanotube; CVD, chemical vapor deposition; DC, direct current; DGEBA, diglycidyl ether of bisphenol A; FWHM, full width at half maximum; NMP, *N*-methyl-2-pyrrolidone; RTM, resin transfer molding; SAXS, small angle X-ray scattering; WAXS, wide angle X-ray scattering.

REFERENCES

(1) Vigolo, B.; Penicaoud, A.; Coulon, C.; Sauder, C.; Pailler, R.; Journet, C.; Bernier, P.; Poulin, P. Macroscopic Fibers and Ribbons of Oriented Carbon Nanotubes. *Science* **2000**, *290*, 1331–1334.

(2) Li, Y.-L.; Kinloch, I. A.; Windle, A. H. Direct Spinning of Carbon Nanotube Fibers from Chemical Vapor Deposition Synthesis. *Science* **2004**, *304*, 276–278.

(3) Zhang, M.; Atkinson, K. R.; Baughman, R. H. Multifunctional Carbon Nanotube Yarns by Downsizing an Ancient Technology. *Science* **2004**, *306*, 1358–1361.

(4) Vilatela, J. J.; Windle, A. H. Yarn-Like Carbon Nanotube Fibers. *Adv. Mater.* **2010**, *22*, 4959–4963.

(5) Qiu, J.; Terrones, J.; Vilatela, J. J.; Vickers, M. E.; Elliott, J. A.; Windle, A. H. Liquid Infiltration into Carbon Nanotube Fibers: Effect on Structure and Electrical Properties. *ACS Nano* **2013**, *7*, 8412–8422.

(6) Vilatela, J. J.; Khare, R.; Windle, A. H. The Hierarchical Structure and Properties of Multifunctional Carbon Nanotube Fibre Composites. *Carbon N. Y.* **2012**, *50*, 1227–1234.

(7) Mora, R. J.; Vilatela, J. J.; Windle, A. H. Properties of Composites of Carbon Nanotube Fibres. *Compos. Sci. Technol.* **2009**, *69*, 1558–1563.

(8) Lima, M. D.; Fang, S.; Lepro, X.; Lewis, C.; Ovalle-Robles, R.; Carretero-Gonzalez, J.; Castillo-Martinez, E.; Kozlov, M. E.; Oh, J.; Rawat, N.; *et al.* Biscrolling Nanotube Sheets and Functional Guests into Yarns. *Science* **2011**, *331*, 51–55.

(9) Lepró, X.; Ovalle-Robles, R.; Lima, M. D.; Elías, A. L.; Terrones, M.; Baughman, R. H. Catalytic Twist-Spun Yarns of Nitrogen-Doped Carbon Nanotubes. *Adv. Funct. Mater.* **2012**, *22*, 1069–1075.

(10) Dalton, A. B.; Collins, S.; Muñoz, E.; Razal, J. M.; Ebron, V. H.; Ferraris, J. P.; Coleman, J. N.; Kim, B. G.; Baughman, R. H. Super-Tough Carbon-Nanotube Fibres. *Nature* **2003**, *423*, 703–703.

(11) Bogdanovich, A. E.; Bradford, P. D. Carbon Nanotube Yarn and 3-D Braid Composites. Part I: Tensile Testing and Mechanical Properties Analysis. *Compos. Part A Appl. Sci. Manuf.* **2010**, *41*, 230–237.

(12) Valentini, L.; Armentano, I.; Kenny, J. M.; Cantalini, C.; Lozzi, L.; Santucci, S. Sensors for Sub-Ppm NO2 Gas Detection Based on Carbon Nanotube Thin Films. *Appl. Phys. Lett.* **2003**, *82*, 961.

(13) Slobodian, P.; Riha, P.; Lengalova, A.; Svoboda, P.; Saha, P. Multi-Wall Carbon Nanotube Networks as Potential Resistive Gas Sensors for Organic Vapor Detection. *Carbon N. Y.* **2011**, *49*, 2499–2507.

(14) Foroughi, J.; Spinks, G. M.; Wallace, G. G.; Oh, J.; Kozlov, M. E.; Fang, S.; Mirfakhrai, T.; Madden, J. D. W.; Shin, M. K.; Kim, S. J.; *et al.* Torsional Carbon Nanotube Artificial Muscles. *Science* **2011**, *334*, 494–497.

(15) Lima, M. D.; Li, N.; Jung de Andrade, M.; Fang, S.; Oh, J.; Spinks, G. M.; Kozlov, M. E.; Haines, C. S.; Suh, D.; Foroughi, J.; *et al.* Electrically, Chemically, and Photonically Powered Torsional and Tensile Actuation of Hybrid Carbon Nanotube Yarn Muscles. *Science* **2012**, *338*, 928–932.

(16) Zhao, Y.; Wei, J.; Vajtai, R.; Ajayan, P. M.; Barrera, E. V. Iodine Doped Carbon Nanotube Cables Exceeding Specific Electrical Conductivity of Metals. *Sci. Rep.* **2011**, *1*, 83.

(17) Subramaniam, C.; Yamada, T.; Kobashi, K.; Sekiguchi, A.; Futaba, D. N.; Yumura, M.; Hata, K. One Hundred Fold Increase in Current Carrying Capacity in a Carbon Nanotube-Copper Composite. *Nat. Commun.* **2013**, *4*, 2202.

(18) Cheng, H.; Dong, Z.; Hu, C.; Zhao, Y.; Hu, Y.; Qu, L.; Chen, N.; Dai, L. Textile Electrodes Woven by Carbon Nanotube-Graphene Hybrid Fibers for Flexible Electrochemical Capacitors. *Nanoscale* **2013**, *5*, 3428–3434.

(19) Xu, P.; Gu, T.; Cao, Z.; Wei, B.; Yu, J.; Li, F.; Byun, J.-H.; Lu, W.; Li, Q.; Chou, T.-W. Carbon Nanotube Fiber Based Stretchable Wire-Shaped Supercapacitors. *Adv. Energy Mater.* **2014**, *4*, n/a–n/a.

(20) Reguero, V.; Alemán, B.; Mas, B.; Vilatela, J. J. Controlling Carbon Nanotube Type in Macroscopic Fibers Synthesized by the Direct Spinning Process. *Chem. Mater.* **2014**, *26*, 3550–3557.

(21) Elliott, J.; Sandler, J.; Windle, A.; Young, R.; Shaffer, M. Collapse of Single-Wall Carbon Nanotubes Is Diameter Dependent. *Phys. Rev. Lett.* **2004**, *92*, 095501.

(22) Motta, M.; Moisala, A.; Kinloch, I. A.; Windle, A. H. High Performance Fibres from "Dog Bone" Carbon Nanotubes. *Adv. Mater.* **2007**, *19*, 3721–3726.

(23) Gspann, T. S.; Smail, F. R.; Windle, A. H. FD173: Spinning of Carbon Nanotube Fibres Using the Floating Catalyst High Temperature Route: Purity Issues and the Critical Role of Sulphur. *Faraday Discuss.* **2014**. Published online, DOI: 10.1039/c4fd00066h.

(24) Nirmalraj, P. N.; Lyons, P. E.; De, S.; Coleman, J. N.; Boland, J. J. Electrical Connectivity in Single-Walled Carbon Nanotube Networks. *Nano Lett.* **2009**, *9*, 3890–3895.

(25) Motta, M.; Kinloch, I.; Moisala, A.; Premnath, V.; Pick, M.; Windle, A. The Parameter Space for the Direct Spinning of Fibres and Films of Carbon Nanotubes. *Phys. E Low-dimensional Syst. Nanostructures* **2007**, *37*, 40–43.

(26) Haynes, W. M. *CRC Handbook of Chemistry and Physics*; Haynes, W. M., Ed.; 94th ed.; CRC Press: Boca Raton, 2013; pp. 1–2668.

(27) Giaever, I. Tunneling Phenomena in Solids. In; Burstein, E.; Lundqvist, S., Eds.; Springer US: Boston, MA, 1969; pp. 19–30.

(28) Kirkpatrick, S. Percolation and Conduction. *Rev. Mod. Phys.* **1973**, *45*, 574–588.

(29) Bernasconi, J. Electrical Conductivity in Disordered Systems. *Phys. Rev. B* **1973**, *7*, 2252–2260.

(30) Erdös, P.; Haley, S. Random-Network Models of the Conductance of Disordered Condensed Matter. *Phys. Rev. B* **1976**, *13*, 1720–1727.

(31) Naraghi, M.; Filleter, T.; Moravsky, A.; Locascio, M.; Loutfy, R. O.; Espinosa, H. D. A Multiscale Study of High Performance Double-Walled Nanotube−Polymer Fibers. *ACS Nano* **2010**, *4*, 6463–6476.

(32) Rahatekar, S. S.; Shaffer, M. S. P.; Elliott, J. A. Modelling Percolation in Fibre and Sphere Mixtures: Routes to More Efficient Network Formation. *Compos. Sci. Technol.* **2010**, *70*, 356–362.